INTERNATIONAL JOURNAL FOR NUMERICAL METHODS IN ENGINEERING
*Int. J. Numer. Meth. Engng* 2004; **61**:1546–1563
Published online 28 September 2004 in Wiley InterScience (www.interscience.wiley.com). DOI: 10.1002/nme.1127

# Linear eigenvalue analysis of the disc-brake squeal problem

Q. Cao[1], H. Ouyang[1,*,†], M. I. Friswell[2] and J. E. Mottershead[1]

[1]*Department of Engineering, University of Liverpool, Liverpool L69 3GH, U.K.*
[2]*Department of Aerospace Engineering, University of Bristol, Bristol BS8, U.K.*

SUMMARY

This paper presents a numerical method to calculate the unstable frequencies of a car disc brake and suggests a suitable analysis procedure. The stationary components of the disc brake are modelled using finite elements and the disc as a thin plate. The separate treatments of the stationary components and the rotating disc facilitate the modelling of the disc brake squeal as a moving load problem. Some uncertain system parameters of the stationary components and the disc are tuned to fit experimental results. A linear, complex-valued, asymmetric eigenvalue formulation is derived for the friction-induced vibration of the disc brake. Predicted unstable frequencies are compared with experimentally established squeal frequencies of a real car disc brake. Copyright © 2004 John Wiley & Sons, Ltd.

KEY WORDS: disc brake; squeal; vibration; moving loads; friction; numerical method

## 1. INTRODUCTION

Friction-induced vibration and noise emanating from car disc brakes is a source of considerable discomfort and leads to customer dissatisfaction. The high frequency noise above 1 kHz, known as squeal, is most annoying and is very difficult to eliminate. Akay [1] recently reviewed friction-induced noise, including car disc brake squeal. He quoted from an industrial source an estimate of the warranty cost due to noise, harshness and vibration (together known as the NVH problem), including disc brake squeal, as US$ 1 billion a year to the automotive industry in North America alone.

North [2] observed that the first concerted effort to study car disc brake squeal was made at the Motor Industrial Research Association (MIRA) in the U.K. in the 1950s. There now exists an extensive literature on theoretical and experimental investigations of disc brake squeal. To appreciate this very complex problem, reviews [2–5] conducted at different times are recommended. Kinkaid *et al.*'s recent thorough survey [6] deserves a special mention. To date, the

*Correspondence to: H. Ouyang, Department of Engineering, University of Liverpool, Liverpool L69 3GH, U.K.
†E-mail: h.ouyang@Liverpool.ac.uk

Contract/grant sponsor: EPSRC; contract/grant number: GR/L91061
Contract/grant sponsor: TRW Automotive

*Received 4 October 2003*
*Revised 8 January 2004*
*Accepted 20 February 2004*

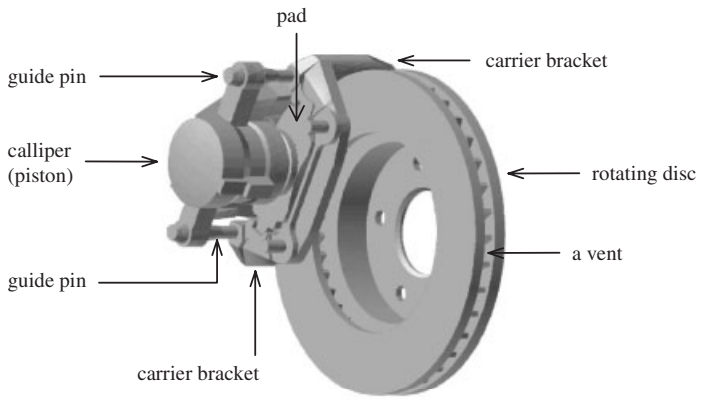


Figure 1. A car disc brake of floating calliper design.

disc brake vibration and squeal problem has not been well solved, even though disc brakes have become quieter over the years.

A car disc brake system consists of a rotating disc and stationary (non-rotating) pads, carrier bracket, calliper and (mounting) guide pins. The pads are loosely housed in the calliper and located by the carrier bracket. The calliper itself is allowed to slide fairly freely along the two mounting guide pins in a floating calliper design. A typical floating-type vented disc brake system is shown in Figure 1. The disc is bolted to the car wheel and thus rotates at the same speed as the wheel. When the disc brake is applied, the two pads are brought into contact with the disc surfaces. Most of the kinetic energy of the travelling car is converted to heat through friction. But a small part of it converts into sound energy and generates noise. A squealing brake is difficult and expensive to correct. Preferably the noise issue should be resolved at the design stage. There are a number of names for brake noises in different frequency ranges. Among these, high frequency noise, or squeal, is the most difficult one to deal with.

In parallel with experimental study, modelling of disc brakes and simulating their dynamics and acoustic behaviour is an efficient way of understanding the squeal mechanism and designing quiet disc brakes. The standard technology in the car manufacturing industry is to use large finite element models. By using a large number of finite elements, an adequate structural model can be established. The remaining issues in modelling are the friction models, the squeal mechanisms, the contact models and the dynamics models.

Most analyses of disc brake squeal adopt simple friction laws since a brake system is very complicated. Various squeal mechanisms have been used, including the negative gradient of friction coefficient against relative speed and the stick-slip vibration studied by Mills [7, 8], the sprag–slip model put forward by Spurr [9], North's follower force and friction couple [2], the rotating follower force advanced by Mottershead and co-workers [10, 11], and so on.

Some recent finite element analyses also contain a static contact analysis of the contact area and the pressure distribution of the disc/pads interface [12–14]. Some even embarked on a dynamic contact analysis to consider the making and breaking of contact between the disc and the pads [15].

 

The authors think that the dynamics models for the disc brake squeal need further improvement. In a disc brake system, the disc rotates past the stationary pads housed by the carrier bracket and the calliper. As a result, the pads mate with different spatial areas as the disc rotates and vibrates. This is a moving load problem. Because disc brakes tend to squeal at low speeds, the moving load nature of the problem has been omitted until very recently. Ouyang *et al.* [16] conceptually divided a disc brake into the rotating disc and the stationary components, and put forward an analytical-numerical combined approach for analysing disc brake vibration and squeal. They cast the disc brake vibration and squeal as a moving load problem and adopted the analysis strategy presented in Reference [17]. The separate treatment of the disc and the stationary components greatly facilitates the formulation of the disc brake vibration and squeal as a moving load problem. These two features distinguish the authors' approach from those of other researchers' and will be retained in this paper.

As a first attempt to analyse a disc brake in the light of moving loads, the work reported in Reference [17] led to a highly non-linear eigenvalue formulation, which requires a very time-consuming search method. This search method also needs the analyst's intervention during the search process. There may be a chance that the search would miss a system eigenvalue. One of the main objectives of this paper is to address the above-mentioned problems with the non-linear eigenvalue formulation. A linear eigenvalue formulation is derived and presented. This paper also describes the procedure required to analyse the disc brake squeal of a real car disc brake system and compares the numerical predictions to experimental results.

## 2. EQUATION OF MOTION OF THE DISC

The disc in a disc brake system is a top-hat like structure, whose top is bolted to the wheel. The annulus part can be solid or have many ventilation holes. The finite element analysis of the disc studied in this paper indicates that there are more out-of-plane frequencies than in-plane frequencies under 20 kHz. The low frequency squeal was defined as the range of frequency below the first in-plane squeal frequency of a disc brake system [18]. The low frequency squeal (between 1 and 6 kHz) is the topic of this paper. As such, the in-plane motion of the disc is omitted. The brake disc consists of three parts: the top, the cylindrical wall and the annulus that is in contact with the pads. The top of the disc has the same number of axes of cyclic symmetry as the number of bolt holes (usually four or five). The cylindrical part of the disc is axially symmetric. The annulus is axially symmetric for a solid disc and is cyclically symmetric for a vented disc. An axially symmetric disc possesses a number of double natural frequencies and modes with the same number of nodal diameters. A real brake disc, though not possessing double frequencies, has pairs of rather close frequencies, each of which corresponds to modes with the same number of nodal diameters. In this paper, the brake disc is approximated as an annular plate (perfectly axially symmetric).

The brake disc is subjected to a number of normal and tangential friction forces at the disc/pads interface from the pads, as illustrated in Figure 2. Each friction force acting on the top or bottom surface of the disc produces a bending couple about the mid-plane of the disc as

$$M_i = \mu_i p_i h/2 \tag{1}$$

 

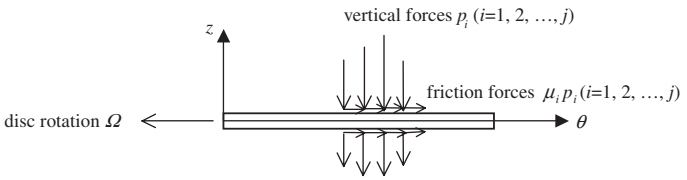


Figure 2. The forces acting onto the disc from the pads.

on the $i$th contact node at the polar co-ordinate of $(r_i, \theta_i)$ on the disc/pads interface at time $t = 0$ (when sliding starts). Friction manifested in this way was first proposed by North for a rigid disc model [2] and recently extended to a beam model of the disc by Hulten and Flint [19]. Equation (1) adopts the simple Coulomb friction law that is used in the present study. The formulation in this paper allows friction coefficient to be a function of the disc speed $\Omega$ and to vary from node to node, though it is used as a constant in the present work. Note also that the friction coefficients for the bottom surface of the disc take negative values.

The equation of transverse motion of the annular plate (as a substitute for the disc), which is subjected to a number of rotating concentrated normal forces and bending couples, is

$$\rho h \frac{\partial^2 w}{\partial t^2} + c \frac{\partial w}{\partial t} + D\nabla^4 w = -\frac{1}{r} \sum_{i=1}^{j} \left\{ p_i(t)\delta(\theta - \theta_i - \Omega t) + \frac{\partial}{r\partial\theta}[M_i(t)\delta(\theta - \theta_i - \Omega t)] \right\} \delta(r - r_i) \tag{2}$$

where

$$\nabla^4 = \left( \frac{\partial^2}{\partial r^2} + \frac{1}{r}\frac{\partial}{\partial r} + \frac{1}{r^2}\frac{\partial^2}{\partial \theta^2} \right)^2 \tag{3}$$

Some of the essential steps of the derivation reported in Reference [17] are now repeated here for the sake of completeness. Those symbols not explained in the text are explained in Appendix A.

The solution of Equation (2) can be expressed as

$$w(r, \theta, t) = \sum_{m=0}^{\infty} \sum_{n=-\infty}^{\infty} \psi_{mn}(r, \theta) q_{mn}(t) \tag{4}$$

where the mode shape functions of the unloaded plate

$$\psi_{mn}(r, \theta) = \frac{R_{mn}(r)}{\sqrt{\rho h b^2}} \exp(\mathrm{i}n\theta) \quad (m = 0, 1, 2, \ldots;\ n = 0, \pm 1, \pm 2, \ldots) \tag{5}$$

 

satisfy the ortho-normality conditions,

$$\int_0^{2\pi}\int_a^b \rho h\bar{\psi}_{kl}\psi_{mn} r\,\mathrm{d}r\,\mathrm{d}\theta = \delta_{km}\delta_{ln}, \qquad \int_0^{2\pi}\int_a^b D\bar{\psi}_{kl}\nabla^4\psi_{mn} r\,\mathrm{d}r\,\mathrm{d}\theta = \omega_{mn}^2\delta_{km}\delta_{ln}$$
$$(k = 0, 1, 2, \ldots; l = 0, \pm1, \pm2, \ldots) \tag{6}$$

where the bar over a symbol denotes complex conjugation. The modes of an annular plate are in the form of nodal diameters and nodal circles. Pure nodal circle modes are single modes while modes involving nodal diameters are double modes.

Substituting Equations (4) and (5) into Equation (2) and making use of Equation (6) yields

$$\ddot{q}_{kl} + 2\xi\omega_{kl}\dot{q}_{kl} + \omega_{kl}^2 q_{kl} = -\frac{1}{\sqrt{\rho h b^2}}\sum_i^j R_{kl}(r_i)\,\exp[-\mathrm{i}l(\theta_i + \Omega t)]\left(1 - \frac{\mu_i h}{2r_i}\,\mathrm{i}l\right)p_i$$
$$(l = 0, \pm1, \pm2, \ldots) \tag{7}$$

Equation (7) may be re-written in matrix form as

$$\mathbf{D}\mathbf{q} = -\mathrm{diag}[\exp(-\mathrm{i}l\Omega t)]\mathbf{S}'^{\mathrm{H}}\mathbf{p} \tag{8}$$

where

$$\mathbf{D} = \mathrm{diag}\left[\frac{\mathrm{d}^2}{\mathrm{d}t^2} + 2\xi\omega_{kl}\frac{\mathrm{d}}{\mathrm{d}t} + \omega_{kl}^2\right]$$
$$= \begin{bmatrix} \frac{\mathrm{d}^2}{\mathrm{d}t^2} + 2\xi\omega_{00}\frac{\mathrm{d}}{\mathrm{d}t} + \omega_{00}^2 & & & \\ & \frac{\mathrm{d}^2}{\mathrm{d}t^2} + 2\xi\omega_{01}\frac{\mathrm{d}}{\mathrm{d}t} + \omega_{01}^2 & & \\ & & \frac{\mathrm{d}^2}{\mathrm{d}t^2} + 2\xi\omega_{0,-1}\frac{\mathrm{d}}{\mathrm{d}t} + \omega_{0,-1}^2 & \\ & & & \ddots \end{bmatrix} \tag{9}$$

the element of the matrix $\mathbf{S}'$ at the $i$th row and $m$th column is

$$\mathbf{S}'(i, m) = \frac{R_{km}(r_i)}{\sqrt{\rho h b^2}}\,\exp(\mathrm{i}m\theta_i)\left(1 + \frac{\mu_i h}{2r_i}\,\mathrm{i}m\right) \tag{10}$$

 

the superscript H denotes the conjugate transpose, and

$$\mathrm{diag}[\exp(-\mathrm{i}l\Omega t)] = \begin{bmatrix} 1 & & & & & & \\ & \exp(-\mathrm{i}\Omega t) & & & & & \\ & & \exp(\mathrm{i}\Omega t) & & & & \\ & & & \exp(-\mathrm{i}2\Omega t) & & & \\ & & & & \exp(\mathrm{i}2\Omega t) & & \\ & & & & & \ddots & \\ & & & & & & \ddots \end{bmatrix}$$

$$= \{\mathrm{diag}[\exp(\mathrm{i}l\Omega t)]\}^{-1}$$

## 3. EQUATION OF MOTION OF THE STATIONARY COMPONENTS

The stationary components of a disc brake, as seen from Figure 1, are very complicated in geometry. They have to be described by many finite elements. An industrial finite element model of the stationary components of a disc brake may have over 100 000 degrees-of-freedom. There is a time penalty with these very detailed finite element models. To increase computational efficiency, substructuring or superelements are used. In the present work, the Craig-Bampton dynamic reduction technique is used to reduce the large finite element model of the stationary components to a much smaller, suitable finite element model.

Another complexity of a disc brake system is the presence of a number of contact interfaces between any two stationary components because of the way they are assembled. The interface between the pads and the disc is the most important one and should be modelled carefully. When the brake is applied, the asperities on the disc surfaces and on the pad surfaces are squashed under high local pressure and hence form a layer of material that is different from the disc and pad materials. Here a thin layer of solid elements is used. This is treated as an orthotropic material that has a very high Young's modulus in the normal direction and relatively small Young's moduli in the other two directions (i.e. the tangential plane). These Young's moduli may vary from element to element and are assumed to depend on the local pressures, which are determined through a non-linear, static contact analysis [20]. Other researchers, for example [12, 13], used spring elements for this contact. In the present contact analysis, the disc is assumed to be rigid and the pads are allowed to slide on the disc surface. Once the pressure distribution is found, the local, element-wise Young's moduli can be determined if the pressure-dependence of the pad material properties is known. The local friction coefficients at each node on the disc/pads interface may also be specified from the corresponding nodal, normal forces should the relationship between the two quantities have been established.

When the stationary components of a disc brake are considered as a separate part of a disc brake, the disc and pads interface becomes a free boundary with unknown forces and

 

displacements. The equation of motion of the reduced finite element model of the stationary components is

$$\mathbf{M}\ddot{\mathbf{x}} + \mathbf{C}\dot{\mathbf{x}} + \mathbf{K}\mathbf{x} = \mathbf{f} \tag{11}$$

The matrices in the above equation are partitioned into two parts, one for the displacements at the contact nodes at the disc/pads interface and one for the displacements of the other nodes. The displacements at these contact nodes are further divided into three subsets (vectors) for $u$, $v$ and $w$ displacements respectively. Equation (11), when partitioned, then becomes

$$\begin{bmatrix} \mathbf{D}_{\mathrm{p},uu} & \mathbf{D}_{\mathrm{p},uv} & \mathbf{D}_{\mathrm{p},uw} & \mathbf{D}_{\mathrm{po},u} \\ \mathbf{D}_{\mathrm{p},vu} & \mathbf{D}_{\mathrm{p},vv} & \mathbf{D}_{\mathrm{p},vw} & \mathbf{D}_{\mathrm{po},v} \\ \mathbf{D}_{\mathrm{p},wu} & \mathbf{D}_{\mathrm{p},wv} & \mathbf{D}_{\mathrm{p},ww} & \mathbf{D}_{\mathrm{po},w} \\ \mathbf{D}_{\mathrm{op},u} & \mathbf{D}_{\mathrm{op},v} & \mathbf{D}_{\mathrm{op},w} & \mathbf{D}_{\mathrm{oo}} \end{bmatrix} \begin{Bmatrix} \mathbf{u}_{\mathrm{p}} \\ \mathbf{v}_{\mathrm{p}} \\ \mathbf{w}_{\mathrm{p}} \\ \mathbf{x}_{\mathrm{o}} \end{Bmatrix} = \begin{Bmatrix} 0 \\ \boldsymbol{\mu}\mathbf{p} \\ \mathbf{p} \\ 0 \end{Bmatrix} \tag{12}$$

where

$$\mathbf{D}_{\mathrm{a},b} = \mathbf{M}_{\mathrm{a},b}\frac{\mathrm{d}^2}{\mathrm{d}t^2} + \mathbf{C}_{\mathrm{a},b}\frac{\mathrm{d}}{\mathrm{d}t} + \mathbf{K}_{\mathrm{a},b}, \quad \boldsymbol{\mu} = \begin{bmatrix} \mu_1 & & & & \\ & \mu_2 & & & \\ & & \cdot & & \\ & & & \cdot & \\ & & & & \cdot \\ & & & & \mu_j \end{bmatrix} \tag{13}$$

and the first subscript 'a' designates nodes at the disc/pads interface (thus 'p') or other locations (thus 'o'), and the second subscript 'b' denotes the displacement $u$, or $v$ or $w$ in those places represented by 'a', respectively. Note the relative rotation between the disc and the pads take place in the $\theta$ direction only. Therefore the friction forces appear only in the $\theta$ direction only (corresponding to displacement $v$). Disc brake vibration and squeal is induced by the (internal) friction forces at the disc/pads interface. There is no external force involved.

Multiplying the third row in Equation (12) by $\boldsymbol{\mu}$ and subtracting it from the second row gives

$$\begin{bmatrix} \mathbf{D}_{\mathrm{p},uu} & \mathbf{D}_{\mathrm{p},uv} & \mathbf{D}_{\mathrm{p},uw} & \mathbf{D}_{\mathrm{po},u} \\ \mathbf{D}_{\mathrm{p},vu} - \boldsymbol{\mu}\mathbf{D}_{\mathrm{p},wu} & \mathbf{D}_{\mathrm{p},vv} - \boldsymbol{\mu}\mathbf{D}_{\mathrm{p},wv} & \mathbf{D}_{\mathrm{p},vw} - \boldsymbol{\mu}\mathbf{D}_{\mathrm{p},ww} & \mathbf{D}_{\mathrm{po},v} - \boldsymbol{\mu}\mathbf{D}_{\mathrm{po},w} \\ \mathbf{D}_{\mathrm{op},u} & \mathbf{D}_{\mathrm{op},v} & \mathbf{D}_{\mathrm{op},w} & \mathbf{D}_{\mathrm{oo}} \end{bmatrix} \begin{Bmatrix} \mathbf{u}_{\mathrm{p}} \\ \mathbf{v}_{\mathrm{p}} \\ \mathbf{w}_{\mathrm{p}} \\ \mathbf{x}_{\mathrm{o}} \end{Bmatrix} = \begin{Bmatrix} 0 \\ 0 \\ 0 \end{Bmatrix} \tag{14}$$

## 4. DYNAMICS OF THE WHOLE DISC BRAKE SYSTEM

The dynamics of the disc and the stationary components have been established in Sections 2 and 3. Now it is time to construct a dynamic model of the whole system. As mentioned before, the disc rotates past the stationary pads. This moving frictional contact must be duly considered. Therefore the vibration and squeal of disc brakes is cast as a moving load problem.

 

Analytical solutions of many simple moving load problems were calculated by Fryba [21]. The vibration of discs subjected to simple moving loads were first studied by Mote [22] for a stationary disc excited by a rotating load and by Iwan and Moeller [23] for the dual problem of a disc spinning past a stationary load, without any friction. A friction force modelled as a follower force was introduced by Ono *et al.* for a pin-on-spinning disc problem [24] and by Chan *et al.* for a rotating-pin-on-disc problem [10]. The vibration and dynamic stability of discs were reviewed by Mottershead [25].

This investigation is interested in the dynamics of the disc at very low rotational speeds (below about 15 radians/s), where squeal tends to occur, and where gyroscopic and centrifugal effects are very small and can be neglected. A cylindrical co-ordinate system fixed to the centre of the plate is used to describe the transverse plate vibration. The stationary components are then considered as moving relative to the disc. At the disc/pads interface, it is assumed that the $w$-displacements of the pads equal the transverse deflections of the annular plate. Taking into account the relative motion of the disc at a constant rotating speed, the displacement continuity condition at the disc/pads interface (when the pads are moving in the $\theta$ direction) is

$$\mathbf{w}_{\mathrm{p}} = \{w(r_1, \theta_1 + \Omega t, t), w(r_2, \theta_2 + \Omega t, t), \ldots\ldots, w(r_j, \theta_j + \Omega t, t)\}^{\mathrm{T}} \tag{15}$$

Since

$$w(r_i, \theta_i + \Omega t, t) = \frac{1}{\sqrt{\rho h b^2}} \sum_{m=0}^{\infty} \sum_{n=-\infty}^{\infty} R_{mn}(r_i) \exp[\mathrm{i}n(\theta_i + \Omega t)] q_{mn}(t) \quad (i = 1, 2, \ldots, j) \tag{16}$$

it follows that

$$\mathbf{w}_{\mathrm{p}} = \mathbf{S}\,\mathrm{diag}[\exp(\mathrm{i}n\Omega t)]\mathbf{q} \tag{17}$$

where the element of the matrix $\mathbf{S}$ at the $i$th row and the $m$th column is

$$\mathbf{S}(i, m) = \frac{R_{km}(r_i)}{\sqrt{\rho h b^2}} \exp(\mathrm{i}m\theta_i) \tag{18}$$

Equations (8), (14) and (17) provide the means of solving $\mathbf{u}_{\mathrm{p}}$, $\mathbf{v}_{\mathrm{p}}$, $\mathbf{w}_{\mathrm{p}}$ and $\mathbf{q}$. However, the second order differential equation (8) does not allow an explicit solution to be found. In the authors' previous work, a solution in the form of an exponential function was assumed and in the end a highly non-linear eigenvalue formulation was derived. In the present study, an efficient algorithm is sought. The breakthrough comes from the inherent structure of the mathematics involved. A close examination of Equations (8) and (17) reveals that the diagonal matrices represented by diag (exponential in the time domain) in these two equations are inverses of each other. Moreover, the left-hand side differential operator $\mathbf{D}$ in Equation (8) is also a diagonal matrix. This finding affords a solution to these complicated equations as follows.

Let

$$\mathbf{q} = \mathrm{diag}[\exp(-\mathrm{i}n\Omega t)]\mathbf{y} \tag{19}$$

where $\mathbf{y}$ is a new vector. Substitute Equation (19) into (8) and remove the identical diagonal matrix of the exponential function of $t$ on both sides of the resultant equation. This transforms Equation (8) into

$$\mathbf{D}'\mathbf{y} = -\mathbf{S}'^{\mathrm{H}}\mathbf{p} \tag{20}$$

 

where

$$\mathbf{D}' = \operatorname{diag}\left[\left(\frac{\mathrm{d}}{\mathrm{d}t} - \mathrm{i}l\Omega\right)^2 + 2\xi\omega_{kl}\left(\frac{\mathrm{d}}{\mathrm{d}t} - \mathrm{i}l\Omega\right) + \omega_{kl}^2\right]$$

$$= \begin{bmatrix} \dfrac{\mathrm{d}^2}{\mathrm{d}t^2} + 2\xi\omega_{00}\dfrac{\mathrm{d}}{\mathrm{d}t} + \omega_{00}^2 & & & \\ & \left(\dfrac{\mathrm{d}}{\mathrm{d}t} - \mathrm{i}\Omega\right)^2 + 2\xi\omega_{01}\left(\dfrac{\mathrm{d}}{\mathrm{d}t} - \mathrm{i}\Omega\right) + \omega_{01}^2 & & \\ & & \ddots & \\ & & & \ddots \end{bmatrix} \tag{21}$$

Substituting the third row of Equation (12) into Equation (20) gives

$$\mathbf{D}'\mathbf{y} = -\mathbf{S}'^{\mathrm{H}}\begin{bmatrix}\mathbf{D}_{\mathrm{p},wu} & \mathbf{D}_{\mathrm{p},wv} & \mathbf{D}_{\mathrm{p},ww} & \mathbf{D}_{\mathrm{po},w}\end{bmatrix}\begin{Bmatrix}\mathbf{u}_\mathrm{p}\\ \mathbf{v}_\mathrm{p}\\ \mathbf{w}_\mathrm{p}\\ \mathbf{x}_\mathrm{o}\end{Bmatrix} \tag{22}$$

Substituting Equation (19) into (17) allows $\mathbf{w}_\mathrm{p}$ to be expressed by $\mathbf{y}$ as

$$\mathbf{w}_\mathrm{p} = \mathbf{S}\mathbf{y} \tag{23}$$

Now Equation (23) can be substituted into Equations (14) and (22). In so doing, a new matrix differential equation is finally derived as

$$\begin{bmatrix} \mathbf{D}_{\mathrm{p},uu} & \mathbf{D}_{\mathrm{p},uv} & \mathbf{D}_{\mathrm{p},uw}\mathbf{S} & \mathbf{D}_{\mathrm{po},u} \\ \mathbf{D}_{\mathrm{p},vu} - \boldsymbol{\mu}\mathbf{D}_{\mathrm{p},wu} & \mathbf{D}_{\mathrm{p},vv} - \boldsymbol{\mu}\mathbf{D}_{\mathrm{p},wv} & (\mathbf{D}_{\mathrm{p},vw} - \boldsymbol{\mu}\mathbf{D}_{\mathrm{p},ww})\mathbf{S} & \mathbf{D}_{\mathrm{po},v} - \boldsymbol{\mu}\mathbf{D}_{\mathrm{po},w} \\ \mathbf{D}_{\mathrm{op},u} & \mathbf{D}_{\mathrm{op},v} & \mathbf{D}_{\mathrm{op},w}\mathbf{S} & \mathbf{D}_{\mathrm{oo}} \\ \mathbf{S}'^{\mathrm{H}}\mathbf{D}_{\mathrm{p},wu} & \mathbf{S}'^{\mathrm{H}}\mathbf{D}_{\mathrm{p},wv} & \mathbf{D}' + \mathbf{S}'^{\mathrm{H}}\mathbf{D}_{\mathrm{p},ww}\mathbf{S} & \mathbf{S}'^{\mathrm{H}}\mathbf{D}_{\mathrm{po},w} \end{bmatrix}\begin{Bmatrix}\mathbf{u}_\mathrm{p}\\ \mathbf{v}_\mathrm{p}\\ \mathbf{y}\\ \mathbf{x}_\mathrm{o}\end{Bmatrix} = 0 \tag{24}$$

Equation (24) has the dimension of the number of retained degrees-of-freedom of the stationary components (with free boundary at the disc/pads interface) plus the number of the retained modes of the unloaded plate minus the number of contact nodes at the disc/pads interface. It should be noted that there is no restriction on the form of the damping matrix of the stationary components. Therefore $\mathbf{C}$ can be non-proportional and this offers a way of prescribing a more realistic damping model. The whole matrix in Equation (24) is complex-valued and asymmetric. It is also quite large even though a reduced finite element model through substructuring is used. As a second order differential equation, Equation (24) is converted to an expanded first-order

 

differential equation so that the system eigenvalues may be solved. The derivation is given in Appendix B.

## 5. THE PROCEDURE FOR STUDYING DISC BRAKE SQUEAL

The study of the vibration and squeal of a car disc brake is a very complicated procedure, which is briefly summarised as follows.

(1) Conduct modal testing of individual components of the brake to obtain their natural frequencies and modes.
(2) Tune the analytical plate model of the disc to fit the experimental natural frequencies and modes of the disc. Tune the finite element models of the other brake components similarly.
(3) Calculate the modes and frequencies of the unloaded plate analytically.
(4) Non-squeal test: conduct modal testing of the whole disc brake system with the disc brake applied but without disc rotation.
(5) Squeal test: conduct modal testing of the whole disc brake system with the disc brake applied and disc being rotated.
(6) Construct a detailed finite element model for the stationary components. Contacts between the stationary components are considered. A layer of solid elements is installed at the disc/pads interface.
(7) Carry out non-linear static, sliding contact analysis for the disc/pads interface to determine the interfacial pressure distribution and the contact area. This information is then used to specify (partially) the Young's modulus of the contact layer.
(8) Tune the whole disc brake without disc rotation to the experimental natural frequencies and modes of the same structure. This allows a number of uncertain parameters, such as the stiffness of the brake fluid and the Young's modulus of the contact layer at the disc/pads interface, to be determined.
(9) For the fully tuned disc brake system, form the mass, damping and stiffness matrices of the stationary components using a commercial software package.
(10) Compute the mass, damping and stiffness matrices of the reduced finite element model of the stationary components.
(11) Assemble the complex matrices given in Equation (A2) in the appendix from the information obtained in Steps (9) and (10).
(12) Solve the eigenvalue problem defined by Equation (A2).

## 6. NUMERICAL ANALYSIS AND DISCUSSION

The brake disc studied in this paper has the following dimensions and properties: $a = 0.045\,\mathrm{m}$, $b = 0.133\,\mathrm{m}$, $h = 0.012\,\mathrm{m}$, $v = 0.211$, $E = 1.2 \times 10^5\,\mathrm{MPa}$, $\rho = 7200\,\mathrm{kg\,m^{-3}}$. The tuning parameters of the disc model are the spring constants of the elastic boundary conditions at the inner radius $a$ and an equivalent plate thickness. Nineteen natural frequencies of the unloaded plate are calculated by an analytical method and are given in Table I. Numerical natural frequencies from the finite element model of the brake disc shown in Figure 3, which was already tuned and considered to be accurate, are also given in Table I. Due to the asymmetry

 

Table I. Numerical natural frequencies in Hz of the disc.

| $k, l$ | $0, 0$ | $0, \pm1$ | $0, \pm2$ | $0, \pm3$ | $0, \pm4$ | $0, \pm5$ | $0, \pm6$ | $0, \pm7$ | $0, \pm8$ | $0, \pm9$ |
|---|---|---|---|---|---|---|---|---|---|---|
| Analytical $\omega_{kl}$ | 1145 | 745 | 1199 | 2610 | 4225 | 5909 | 7656 | 9445 | 11278 | 13156 |
| Numerical $\omega_{kl}$ | 1146 | 738 | 1196 | 2608 | 4220 | 5904 | 7651 | 9439 | 11270 | 13145 |
| | | 751 | 1202 | 2610 | 4226 | 5910 | 7653 | 9442 | 11275 | 13153 |

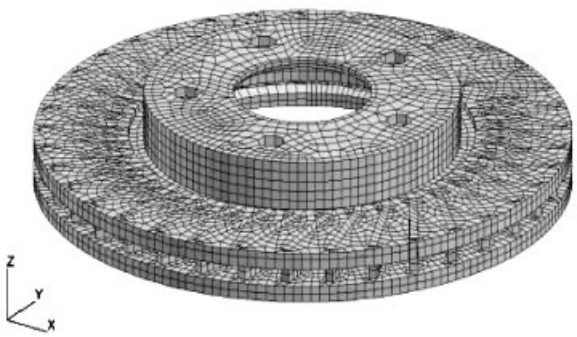


Figure 3. The finite element model of the brake disc.

Table II. Material data of the stationary components.

| Components | Young's | Poisson's ratio | Density (kg m$^{-3}$) |
|---|---|---|---|
| Calliper | 187.63 | 0.3 | 7100 |
| Carrier | 170 | 0.3 | 7564 |
| Back plates, pins | 210 | 0.3 | 7850 |

of the real brake disc, there is a pair of different, albeit very close, numerical frequencies for a diameter mode (there are no double frequencies in a real brake disc or in a finite element model of the real disc). The results in the third row of the table are the pairs of very close numerical frequencies having similar mode shapes (with the same number of nodal circles and the same number of nodal diameters).

Among the nineteen numerical frequencies, eighteen are double frequencies while one is a single frequency (for the $(0, 0)$ mode). Nineteen plate modes are involved in the subsequent computation of the eigenvalues of the whole disc brake system. The highest natural frequency of the unloaded plate involved is 13156 Hz, which is far beyond the range of squeal frequencies of interest and thus is more than satisfactory. Table I indicates that when tuned the annular plate is a good model of the brake disc in the frequency range of interest. It also reveals that the brake disc behaves very much like a perfectly axially symmetric plate despite its asymmetry.

The material properties of the stationary components, except those of the pads, are summarized in Table II.

The pads are constructed with non-linear, viscoelastic material with orthotropic properties. Here they are taken to be linear, elastic and orthotropic but their Young's modulus depends on

 

Table III. A brief summary of the tuned parameters.

| Tuned parameters | Strong influence on |
|---|---|
| Factor for Young's moduli of the elements for friction layer | 6.9 kHz |
| Brake fluid stiffness | 2.4 and 4.3 kHz |
| Stiffness connecting piston head and back plate in the $z$ direction | 3.3–3.6 kHz |
| Stiffness connecting piston head and back plate in the $\theta$ direction | 1.4 kHz |
| Stiffness of the trailing-edge abutment in the $\theta$ direction | |
| Stiffness of the leading-edge abutment in the $\theta$ direction | |
| Stiffness of the leading-edge abutment in the $r$ direction | |
| Stiffness connecting guide pin with carrier bore in the $z$ direction | |

the piston line pressure and the apparent temperature. This dependency is calculated indirectly by comparing the finite element results to the experimental results of the pads. The Young's modulus is between 5.4 and 10.8 GPa.

In addition to the above material properties, there are other parameters which are not readily available. These include the stiffness of the brake fluid, the tangential stiffness at the interface between the piston head and the pad back plate, the stiffness between the pad back plates and the carrier bracket and the stiffness between the carrier bores and the mounting pins. To determine these less certain parameter values of considerable importance, a combination of stiffness values at those four places are numerically tested. Numerical results are compared with experimental frequencies and mode shapes of the brake. Those values that give a good fit between the numerical and experimental results are chosen as the true parameter values. A brief summary of the tuned parameters is given in Table III. The first column defines the parameters used in tuning and the second indicates which predicted unstable frequency is sensitive to which tuning parameter. A blank cell in the second column means that not a single unstable frequency is sensitive to a particular tuning parameter.

This tuning is a time-consuming process but is considered necessary for building a reliable model and getting credible numerical results. Liles [26] determined the connections between disc brake components by using an iterative process and engineering judgement.

The finite element model of the stationary components is shown in Figure 4. The frequencies of the large finite element model and the reduced model are compared with different numbers of retained modes and retained nodes. In so doing, the right numbers of retained modes and nodes in the reduced model are determined.

As mentioned before, the system eigenvalues with positive real parts obtained from the numerical analysis indicate possible squeal frequencies in practice. The value of $\alpha = \sigma/(\sqrt{\sigma^2 + \omega^2})$ is defined as the noise index, which is thought to be an indicator of squeal propensity [27]. As with any stability analysis, the magnitude of a positive real part or its equivalent indicates only the tendency of divergence (rate of growth) in a particular motion characterised by that mode. The growing motion will finally be limited by the inherent non-linearity in the system and a limit-cycle motion will then emerge. The amplitude of the final limit-cycle motion determines the physical strength of a squeal noise. Nack [13] noted that the meaning of using eigenvalue analysis was to determine the necessary condition for a system to become unstable and grow into a state of limit cycles. He argued that if a mode had a negative real part in the eigenvalue, then the motion would not have the chance to grow into a limit-cycle and thus cause sustained noise. Therefore, for engineering design at present, the complex eigenvalue analysis

 

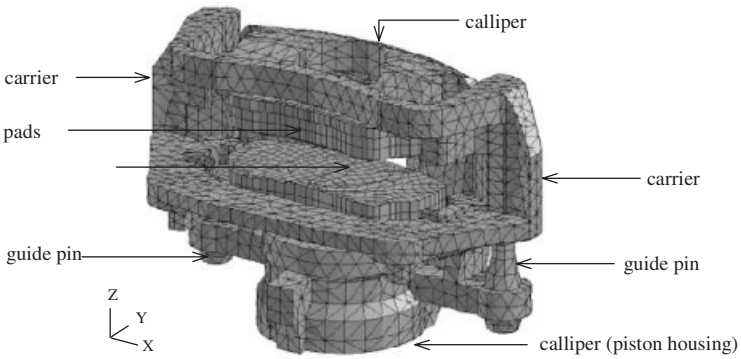


Figure 4. The finite element model of the stationary components.

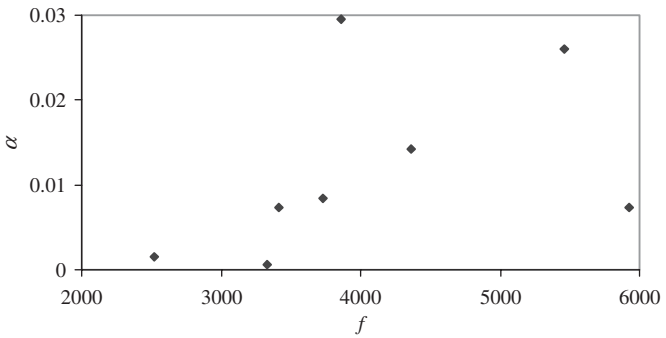


Figure 5. Noise index versus unstable frequency ($\Omega = 0.01$ rad/s).

Table IV. Experimental squeal frequencies.

| | | | | |
|---|---|---|---|---|
| Highest noise level (dB) | 111 | 97 | 95 | 94 |
| Squeal frequency (kHz) | 3.3–3.6 | 4.1 | 2.3 | 5.3–5.5 |

offers a pragmatic approach. Since the limit-cycle motions can only be determined by a very time-intensive transient analysis, it is not an approach favoured by the automotive industry and is not attempted here.

Figures 5 and 6 present noise indices versus frequencies for the predicted unstable eigenvalues. The parameter values used in the above calculation are 0.1% for the damping coefficient of the stationary components, disc damping of $\xi = 0$ and a rather high, constant friction coefficient of $\mu_i = 0.7$.

Experimental results at various low speeds are listed in Table IV.

By comparing the results in Table III with those in Figures 5 and 6, it can be seen that the experimental squeal frequencies correlate rather well with numerical unstable frequencies at near zero speed, particularly if approximately 200 Hz is added to the experimental values.

 

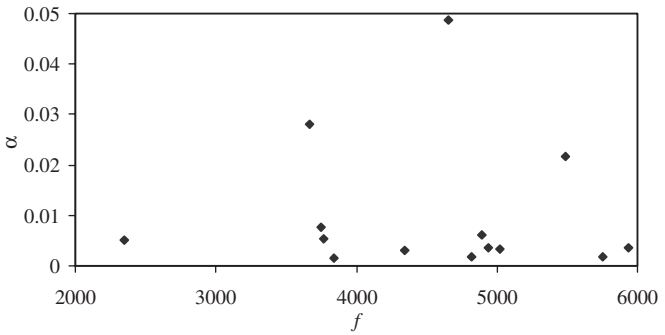


Figure 6. Noise index versus unstable frequency ($\Omega = 6.2$ rad/s).

It should be pointed out that the experiments were conducted on a rig with softer boundary conditions where the disc was bolted to a flexible hub, than those of the plate in the analytical model where it is bolted to a rigid boundary and the in-plane modes were not included.

The first two strong squeal signals are predicted well. The noise levels of the remaining two are less well predicted. In general, the noise indices do not fit as well with experimental noise levels. Note that the noise indices indicate the squeal propensity and not necessarily the noise level, as explained before.

By comparing Figures 5 and 6, one can see that both noise indices and unstable frequencies have undergone significant changes. Notably, the strongest unstable frequency becomes (emerges at) 4653 Hz at the higher disc speed. Notice that the previous strongest and second strongest unstable frequencies at $\Omega = 0.01$ rad/s remain nearly unchanged at the higher speed. Some unstable frequencies around 5 kHz emerge at the higher disc speed.

The numerical results indicate that some strong unstable frequencies and noise indices are speed-dependent. Consideration of moving loads (the case of $\Omega = 6.2$ rad/s) or not (the case of $\Omega = 0.01$ rad/s) indeed makes a big difference in terms of unstable frequencies and the degrees of instability. Friction forces can vary with relative speed in four distinct regimes [28], depending on the magnitude of the normal load applied, but reliable data of this speed dependence for the particular pads and disc contact is not available. Thus, results at other values of $\Omega$ have not been computed. In addition, the software package for the non-linear static contact analysis only distinguished cases of zero and non-zero $\Omega$, and thus results at only two values of $\Omega$ are presented in Figures 5 and 6.

Higher frequencies are not listed for comparison since the numerical results would not be very accurate in the high squeal frequency range when the in-plane motion of the disc is important [18, 29]. The comparison of numerical results with experimental results is made on one particular disc brake system; however it is based on extensive testing including many hundreds of squeal occurrences. To be completely reassured of the methodology more disc brakes would need to be studied.

## 7. CONCLUSIONS

This paper presents a method for modelling car disc brakes and predicting squeal frequencies. The disc brake is treated as a moving load problem consisting of two parts: the rotating disc and

 

the stationary components, which are dealt with respectively by a classical analysis and the finite element method. A plausible squeal mechanism for inducing dynamic instability is incorporated into the model. The unstable frequencies of the disc brake are obtained from a linear, complex-valued, asymmetric eigenvalue formulation established in the paper. The predicted unstable frequencies show a good agreement with the experimentally established squeal frequencies.

## APPENDIX A

Substituting

$$\{\mathbf{u}_\mathrm{p}, \mathbf{v}_\mathrm{p}, \mathbf{y}, \mathbf{x}_\mathrm{o}, \dot{\mathbf{u}}_\mathrm{p}, \dot{\mathbf{v}}_\mathrm{p}, \dot{\mathbf{y}}, \dot{\mathbf{x}}_\mathrm{o}\} = \exp(\lambda t)\mathbf{z}^\mathrm{T} \tag{A1}$$

into Equation (24) and re-arranging the resultant equation gives

$$\left( \begin{bmatrix} 0 & 0 & 0 & 0 & -\mathbf{I} & 0 & 0 & 0 \\ 0 & 0 & 0 & 0 & 0 & -\mathbf{I} & 0 & 0 \\ 0 & 0 & 0 & 0 & 0 & 0 & -\mathbf{I} & 0 \\ 0 & 0 & 0 & 0 & 0 & 0 & 0 & -\mathbf{I} \\ \mathbf{K}_{\mathrm{p},uu} & \mathbf{K}_{\mathrm{p},uv} & \mathbf{K}_{\mathrm{p},uw}\mathbf{S} & \mathbf{K}_{\mathrm{po},u} & \mathbf{C}_{\mathrm{p},uu} & \mathbf{C}_{\mathrm{p},uv} & \mathbf{C}_{\mathrm{p},uw}\mathbf{S} & \mathbf{C}_{\mathrm{po},u} \\ \mathbf{K}_1 & \mathbf{K}_2 & \mathbf{K}_3 & \mathbf{K}_4 & \mathbf{C}_1 & \mathbf{C}_2 & \mathbf{C}_3 & \mathbf{C}_4 \\ \mathbf{K}_{\mathrm{op},u} & \mathbf{K}_{\mathrm{op},v} & \mathbf{K}_{\mathrm{op},w}\mathbf{S} & \mathbf{K}_{\mathrm{oo}} & \mathbf{C}_{\mathrm{op},u} & \mathbf{C}_{\mathrm{op},v} & \mathbf{C}_{\mathrm{op},w}\mathbf{S} & \mathbf{C}_{\mathrm{oo}} \\ \mathbf{K}_5 & \mathbf{K}_6 & \mathbf{K}_7 & \mathbf{K}_8 & \mathbf{C}_5 & \mathbf{C}_6 & \mathbf{C}_7 & \mathbf{C}_8 \end{bmatrix} + \begin{bmatrix} \mathbf{I} & 0 & 0 & 0 & 0 & 0 & 0 & 0 \\ 0 & \mathbf{I} & 0 & 0 & 0 & 0 & 0 & 0 \\ 0 & 0 & \mathbf{I} & 0 & 0 & 0 & 0 & 0 \\ 0 & 0 & 0 & \mathbf{I} & 0 & 0 & 0 & 0 \\ 0 & 0 & 0 & 0 & \mathbf{M}_{\mathrm{p},uu} & \mathbf{M}_{\mathrm{p},uv} & \mathbf{M}_{\mathrm{p},uw}\mathbf{S} & \mathbf{M}_{\mathrm{po},u} \\ 0 & 0 & 0 & 0 & \mathbf{M}_1 & \mathbf{M}_2 & \mathbf{M}_3 & \mathbf{M}_4 \\ 0 & 0 & 0 & 0 & \mathbf{M}_{\mathrm{op},u} & \mathbf{M}_{\mathrm{op},v} & \mathbf{M}_{\mathrm{op},w}\mathbf{S} & \mathbf{M}_{\mathrm{oo}} \\ 0 & 0 & 0 & 0 & \mathbf{M}_5 & \mathbf{M}_6 & \mathbf{M}_7 & \mathbf{M}_8 \end{bmatrix} \lambda \right) \mathbf{z} = 0 \tag{A2}$$

where

$$\mathbf{C}_1 = \mathbf{C}_{\mathrm{p},vu} - \boldsymbol{\mu}\mathbf{C}_{\mathrm{p},wu}, \quad \mathbf{C}_2 = \mathbf{C}_{\mathrm{p},vv} - \boldsymbol{\mu}\mathbf{C}_{\mathrm{p},wv}$$

$$\mathbf{C}_3 = (\mathbf{C}_{\mathrm{p},vw} - \boldsymbol{\mu}\mathbf{C}_{\mathrm{p},ww})\mathbf{S}, \quad \mathbf{C}_4 = \mathbf{C}_{\mathrm{po},v} - \boldsymbol{\mu}\mathbf{C}_{\mathrm{po},w}$$

 

$$\mathbf{K}_1 = \mathbf{K}_{\mathrm{p},vu} - \boldsymbol{\mu}\mathbf{K}_{\mathrm{p},wu}, \quad \mathbf{K}_2 = \mathbf{K}_{\mathrm{p},vv} - \boldsymbol{\mu}\mathbf{K}_{\mathrm{p},wv}$$

$$\mathbf{K}_3 = (\mathbf{K}_{\mathrm{p},vw} - \boldsymbol{\mu}\mathbf{K}_{\mathrm{p},ww})\mathbf{S}, \quad \mathbf{K}_4 = \mathbf{K}_{\mathrm{po},v} - \boldsymbol{\mu}\mathbf{K}_{\mathrm{po},w}$$

$$\mathbf{M}_1 = \mathbf{M}_{\mathrm{p},vu} - \boldsymbol{\mu}\mathbf{M}_{\mathrm{p},wu}, \quad \mathbf{M}_2 = \mathbf{M}_{\mathrm{p},vv} - \boldsymbol{\mu}\mathbf{M}_{\mathrm{p},wv}$$

$$\mathbf{M}_3 = (\mathbf{M}_{\mathrm{p},vw} - \boldsymbol{\mu}\mathbf{M}_{\mathrm{p},ww})\mathbf{S}, \quad \mathbf{M}_4 = \mathbf{M}_{\mathrm{po},v} - \boldsymbol{\mu}\mathbf{M}_{\mathrm{po},w}$$

$$\mathbf{C}_5 = \mathbf{S}'^{\mathrm{H}}\mathbf{C}_{\mathrm{p},wu}, \quad \mathbf{C}_6 = \mathbf{S}'^{\mathrm{H}}\mathbf{C}_{\mathrm{p},wv}, \quad \mathbf{C}_7 = \mathrm{diag}[2(\xi\omega_{kl} - \mathrm{i}l\Omega)] + \mathbf{S}'^{\mathrm{H}}\mathbf{C}_{\mathrm{p},ww}\mathbf{S}$$

$$\mathbf{C}_8 = \mathbf{S}'^{\mathrm{H}}\mathbf{C}_{\mathrm{po},w}$$

$$\mathbf{K}_5 = \mathbf{S}'^{\mathrm{H}}\mathbf{K}_{\mathrm{p},wu}, \quad \mathbf{K}_6 = \mathbf{S}'^{\mathrm{H}}\mathbf{K}_{\mathrm{p},wv}$$

$$\mathbf{K}_7 = \mathrm{diag}[\omega_{kl}^2 - \mathrm{i}2\xi\omega_{kl}l\Omega - l^2\Omega^2] + \mathbf{S}'^{\mathrm{H}}\mathbf{K}_{\mathrm{p},ww}\mathbf{S}, \quad \mathbf{K}_8 = \mathbf{S}'^{\mathrm{H}}\mathbf{K}_{\mathrm{po},w}$$

$$\mathbf{M}_5 = \mathbf{S}'^{\mathrm{H}}\mathbf{M}_{\mathrm{p},wu}, \quad \mathbf{M}_6 = \mathbf{S}'^{\mathrm{H}}\mathbf{M}_{\mathrm{p},wv}$$

$$\mathbf{M}_7 = \mathbf{I} + \mathbf{S}'^{\mathrm{H}}\mathbf{M}_{\mathrm{p},ww}\mathbf{S}, \quad \mathbf{M}_8 = \mathbf{S}'^{\mathrm{H}}\mathbf{M}_{\mathrm{po},w}$$

and $\mathbf{z}$ is a constant vector (the eigenvector).

Equation (A2) presents a linear, complex-valued, asymmetric eigenvalue problem. An in-house program is coded to compute $\lambda$.

## APPENDIX B

| | |
|---|---|
| $a, b$ | inner and outer radii of the annular plate model for the brake disc |
| $\mathbf{C}$ | damping matrix of the finite element model of the stationary components |
| $c$ | viscous damping of the plate |
| $D$ | flexural rigidity of the plate |
| $E$ | Young's modulus of the plate |
| $\mathbf{f}$ | force vector for the finite element model of the stationary components |
| $h$ | thickness of the disc |
| i | $\sqrt{-1}$ |
| $\mathbf{I}$ | identity matrix |
| $j$ | number of nodes on the pads at the disc/pads contact interface |
| $\mathbf{K}$ | stiffness matrix of the finite element model of the stationary components |
| $k, l$ or $m, n$ | number of nodal circles and number of nodal diameters in the mode of the unloaded plate |
| $\mathbf{M}$ | mass matrix of the finite element model of the stationary components |
| $p_i$ | total normal force on the disc of the $i$th contact node at the disc/pads interface during vibration |
| $\mathbf{p}$ | force vector consisting of all $p_i$ |
| $q_{kl}$ | modal co-ordinate for $k$ nodal circles and $l$ nodal diameters for the plate |
| $\mathbf{q}$ | modal co-ordinate vectors for the plate |

 

| | |
|---|---|
| $R_{kl}$ | combination of Bessel functions to represent the mode shape of the plate in the $r$ direction |
| $r$ | radial co-ordinate of the cylindrical co-ordinate system |
| $t$ | time |
| $u, v, w$ | displacements of the finite element model of the stationary components of the brake in the $r, \theta$ and $z$ directions, respectively |
| $\mathbf{u}_p, \mathbf{v}_p, \mathbf{w}_p$ | $u, v, w$ displacement vectors for the contact nodes of the pads at the disc/pads interface |
| $w(r, \theta, t)$ | transverse motion (deflection) of the plate |
| $\mathbf{x}$ | displacement vector corresponding to $\mathbf{f}$ |
| $\mathbf{x}_o$ | displacement vector for the nodes other than the contact nodes at the disc/pads interface |
| $z$ | axial co-ordinate of the cylindrical co-ordinate system |
| $\alpha$ | noise index of an unstable frequency |
| $\delta(\cdot)$ | the Dirac delta function |
| $\delta_{kl}$ | the Kronecker delta |
| $\theta$ | circumferential co-ordinate of the cylindrical co-ordinate system |
| $\lambda$ | eigenvalue of the whole disc brake system, $\lambda = \sigma + \omega \mathrm{i}$ |
| $\mu_i$ | kinetic friction coefficient at the $i$th contact node at the disc/pads interface |
| $v$ | Poisson's ratio of the plate |
| $\xi$ | damping coefficient of the plate |
| $\rho$ | mass-density of the plate |
| $\sigma$ | the real part of a system eigenvalue $\lambda$ |
| $\psi_{kl}$ | mode shape function for the transverse vibration of the plate corresponding to $q_{kl}$ |
| $\Omega$ | constant rotating speed of the disc in radians per second |
| $\omega_{kl}$ | undamped natural frequency corresponding to $q_{kl}$ |
| $\omega$ | the imaginary part (frequency) of a system eigenvalue $\lambda$ |

ACKNOWLEDGEMENTS

The authors are grateful for the support by the Engineering and Physical Sciences Research Council of U.K. (grant number GR/L91061) and TRW Automotive. Dr Simon James of University of Liverpool conducted the experiments that are used in tuning the models for the brake components and the whole brake.

REFERENCES

1. Akay A. Acoustics of friction. *Journal of the Acoustic Society of America* 2002; **111**(4):1525–1548.
2. North NR. Disc brake squeal. *Proceedings of IMechE* 1976; **(C38/76)**:169–176.
3. Crolla DA, Lang AM. Brake noise and vibration—the state of the art. In *Vehicle Technology*, No.18 in Tribology Series, Dawson D, Taylor CM, Godet M (eds). 1991; 165–174.
4. Nishiwaki MR. Review of study on brake squeal. *Japan Society of Automobile Engineering Review* 1990; **11**(4):48–54.
5. Yang S, Gibson RF. Brake vibration and noise: review, comments and proposals. *International Journal of Materials Product Technology* 1997; **12**(4–6):496–513.

 

6. Kinkaid NM, O'Reilly OM, Papadopoulos P. Automotive disc brake squeal: a review. *Journal of Sound and Vibration* 2003; **267**(1):105–166.
7. Mills HR. Brake squeal. Inst. of Automobile Engrs. *Report 9162B*, 1939.
8. Mills HR. Brake squeal. Inst. of Automobile Engrs. *Report 9000B*, 1938.
9. Spurr RT. A theory of brake squeal. *Proceedings of IMechE*, *Auto Division* 1961; (1):33–40.
10. Chan SN, Mottershead JE, Cartmell MP. Parametric resonances at subcritical speeds in discs with rotating frictional loads. *Proceedings of IMechE*, *Journal of Engineering Science* 1994; **208**:417–425.
11. Mottershead JE, Ouyang H, Cartmell MP, Friswell MI. Parametric resonances in an annular disc, with a rotating system of distributed mass and elasticity; and the effects of friction and damping. *Proceedings of Royal Society of London Series A* 1997; **453**:1–19.
12. Lee YS, Brooks PC, Barton DC, Crolla DA. A study of disc brake squeal propensity using parametric finite element model. In *IMechE Conference Transaction*, *European Conference On Noise and Vibration*, 12–13 May 1998; 191–201.
13. Nack WV. Brake squeal analysis by the finite element method. *International Journal of Vehicle Design* 2000; **23**(3/4):263–275.
14. Blaschke P, Tan M, Wang A. On the analysis of brake squeal propensity using finite element method. *SAE Paper 2000-01-2765*, 2000.
15. Hu Y, Nagy LI. Brake squeal analysis using non-linear transient finite element method. *SAE Paper 971610*, 1997.
16. Ouyang H, Mottershead JE, Brookfield DJ, James S, Cartmell MP. A methodology for the determination of dynamic instabilities in a car disc brake. *International Journal of Vehicle Design* 2000; **23**(3/4):241–262.
17. Ouyang H, Mottershead JE. A moving-load model for disc-brake stability analysis. *Transaction of ASME*, *Journal of Vibration and Acoustics* 2003; **125**(1):1–6.
18. Dunlap KB, Riehle MA, Longhouse RE. An investigative overview of automotive disc brake noise. *SAE Paper 1999-01-0142*, 1992.
19. Hulten J, Flint J. Lining-deformation-induced modal coupling as squeal generator in a distributed parameter disc brake model. *Journal of Sound and Vibration* 2002; **254**(1):1–21.
20. Tirovic M, Day AJ. Disc brake interface pressure distribution. *Proceedings of IMechE*, *Journal of Automobile Engineering* 1991; **205**:137–146.
21. Fryba L. *Vibration of Solids and Structures Under Moving Loads*. Noordhoff: Groningen, 1972.
22. Mote CD. Stability of circular plates subjected to moving loads. *Journal of Franklin Institute* 1970; **290**: 329–344.
23. Iwan WD, Moeller TL. The stability of a spinning elastic disc with a transverse load system. *ASME Journal of Applied Mechanics* 1976; **43**:485–496.
24. Ono K, Chen JS, Bogy DB. Stability analysis of the head-disk interface in a flexible disc drive. *ASME Journal of Applied Mechanics* 1991; **58**:1005–1014.
25. Mottershead JE. Vibration and friction-induced instability in discs. *Shock and Vibration Digest* 1998; **30**:14–31.
26. Liles GD. Analysis of disc brake squeal using finite element methods. *SAE Paper 891150*, 1989.
27. Yuan Y. A study of the effects of negative friction-speed slope on brake squeal. *Proceedings of 1995 ASME Design Engineering Conference*, Boston, vol. 3, Part A, 1995; 1135–1162.
28. Kragelski IV, Dobychin MN, Kombalov VS. *Friction and Wear*: *Calculation Methods*. Pergamon Press: Oxford, 1982.
29. Matsuzaki M, Izumihara T. Brake noise caused by longitudinal vibration of the disc rotor. *SAE Paper 930804*, 1993.


 